Journal of Solid State Chemistry **165,** 131–135 (2002)
doi:10.1006/jssc.2001.9514, available online at http://www/idealibrary.com on IDEAL®

Magnetic Properties of $LnMnO_3$ (Ln=Ho, Er, Tm, Yb, and Lu)

K. Yoshii and H. Abe*

*Japan Atomic Energy Research Institute, Mikazuki, Hyogo 679-5148, Japan; and *National Institute for Materials Science, Tsukuba, Ibaraki 305-0047, Japan*

Received September 5, 2001; in revised form January 2, 2002; accepted January 18, 2002

Magnetic data are presented for $LnMnO_3$ (Ln = Ho, Er, Tm, Yb, and Lu) having the hexagonal crystal structure of $P6_3cm$. DC magnetization measurements show that magnetic order is not clearly observed for Ln = Ho–Yb, while an antiferromagnetic transition of the Mn^{3+} moments is found at ~90 K for $LuMnO_3$, where the Lu^{3+} ion has no 4f localized moment. This is ascribed to both the paramagnetism of Ln^{3+} and the suppression of magnetization in the Mn^{3+} sublattices arising from strong antiferromagnetic interactions between Mn^{3+}. Deviation from the Curie–Weiss law at low temperatures indicates the onset of antiferromagnetism. Some magnetization data of Ca-substituted compounds, $Ln_{0.5}Ca_{0.5}MnO_3$, which have the different crystal structure of orthorhombic *Pnma*, are also discussed briefly.

Key Words: **manganese oxide; hexagonal structure; orthorhombic structure; antiferromagnetism.**

INTRODUCTION

Rare earth manganites, $LnMnO_3$, have an orthorhombic perovskite structure (space group *Pnma*) for Ln = La–Dy (1–3). The structure changes to a hexagonal $P6_3cm$ structure for the heavier lanthanides of Ln = Ho–Lu as well as Ln = Y and Sc, containing two-dimensional triangular Mn–O lattices (4–10). A neutron diffraction study for Ln = Ho, Er, Tm, Lu, and Sc revealed that these compounds showed antiferromagnetic transitions of the Mn^{3+} moments with Néel temperatures (T_N) of ~70–130 K, below which a noncollinear 120° spin structure was observed (5). Recently, magnetization and neutron diffraction data were reported for Ln = Y (T_N ~ 70 K) and Sc (T_N ~ 130 K), where the Ln^{3+} ions have no localized moment (6, 7). Only $ScMnO_3$ exhibits weak ferromagnetic behavior below T_N and spin reorientation around 70 K (6,7). Magnetization measurements for Ln = Yb and Lu showed antiferromagnetic transitions at T_N = 82 and 86 K, respectively, where only the Yb^{3+} ion has a localized 4f moment ($4f^{13}$) (8). For the other compounds, to the authors' knowledge no magnetization data have been reported, though thermodynamic properties such as heat capacity have been investigated for some of the systems (9,10). In this paper, magnetic data for Ln = Ho, Er, Tm, Y, and Lu, obtained mainly from DC magnetization measurements, are presented. Ca-substituted compounds $Ln_{0.5}Ca_{0.5}MnO_3$, where the nominal valence of the Mn ions is 3.5+, were also prepared for comparison; their magnetic properties are briefly considered as well. Magnetic properties for such systems have been reported for $Y_{0.5}Ca_{0.5}MnO_3$ (11,12) and $Y_{0.7}Ca_{0.3}MnO_3$ (13), exhibiting charge order below 260 K and spin-glass behavior below 30 K, respectively.

EXPERIMENTAL PROCEDURES

The samples were prepared by a solid-state reaction in air as in the previous works (6,8–10). Stoichiometric mixtures of Ln_2O_3 (Ln = Ho, Er, Tm, Yb, and Lu) and Mn_2O_3 (3N–4N, Soekawa) were thoroughly ground, pressed into pellets and fired in air at 1300°C for 24 h. The firing was repeated two to three times with intermediate grindings. Each compound was prepared twice in a separate run and was confirmed to show reproducible structural and magnetic properties. Actual oxygen content y was found to be 3.02–3.04(2) for $LnMnO_y$, based on the titration method as adopted for some manganites (2, 11, 14–16). The slight excess of oxygen is qualitatively the same tendency as that reported for other $LnMnO_3$ compounds with larger Ln^{3+} ions such as $EuMnO_3$ (14). For convenience, the compounds will be denoted as $LnMnO_3$ hereafter. Their crystal structures were determined by powder X-ray diffraction (XRD) using Cu$K\alpha$ radiation for $2\theta = 10°$–$120°$ with an angle step of 0.04°. The XRD patterns were refined by the Rietveld method using the program RIETAN-2000 (17). Magnetic properties were

0022-4596/02 $35.00

measured using a SQUID magnetometer (Quantum Design MPMS) between 4.5 and 400 K. DC magnetization–temperature (M–T) curves were measured in both field-cooled (FC) and zero-field-cooled (ZFC) modes with the applied fields (H) of 1000 Oe. Though the measurements were also done at the low applied field of 20 Oe, the results were found to be essentially the same. Isothermal magnetization was measured at 4.5 K within the applied fields of $\pm 50\,000$ Oe. AC susceptibilities were measured on heating the samples after zero-field cooling to 4.5 K in the same apparatus with the AC field of 4 Oe. The frequency of the AC field was changed between 0.8 and 800 Hz.

RESULTS AND DISCUSSION

Figure 1 shows the XRD patterns of $HoMnO_3$. The obtained lattice parameters are close to those reported previously (4,5). The $P6_3cm$ structure could be assigned also to all the other compounds. The a- and c-lengths were $\sim$6.137–6.044 and $\sim$11.411–11.371 Å, respectively, all of which were confirmed to be close to those in the previous works (4,5). It was found that both of the values decreased with increasing atomic number of Ln, which is in accord with the lanthanide contraction.

Figure 2a shows the M–T curves measured with $H = 1000$ Oe for $LuMnO_3$. The Lu^{3+} ion ($4f^{14}$) has no $4f$ localized moment. Both of the FC and ZFC curves resemble those in Ref. (8), which exhibit an antiferromagnetic transition at $T_N \sim 90$ K. Inverse magnetization curves followed the Curie–Weiss (CW) law above T_N, which provided an effective paramagnetic moment (μ_P) close to a spin-only Mn^{3+} moment (4.90 μ_B; $S = 2$; $3d^4$) and a Weiss temperature (θ) of ~ -700 K. Considering that its absolute value ($|\theta|$) is much higher than the highest measurement temperature of 400 K, magnetization measurements around 700 K would be necessary in the future. This temperature determined in Ref. (8) is $\theta = -887$ K. These large $|\theta|$ values mean the presence of strong antiferromagnetic coupling between Mn^{3+}, as in $YMnO_3$ ($\theta = -312$ K (7) and -705 K (8)) and $ScMnO_3$ ($\theta = -943$ K (6), -663 K

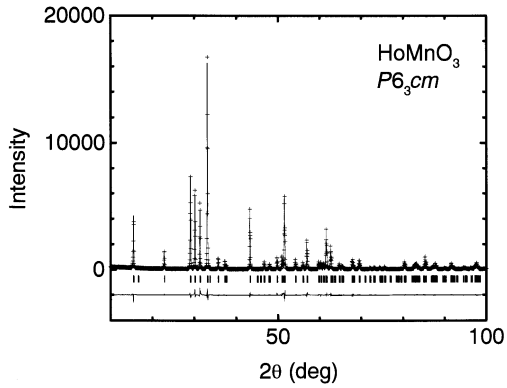

FIG. 1. XRD patterns of $HoMnO_3$ (space group $P6_3cm$, $R_{WP} = 10.27\%$, $R_P = 7.44\%$, $R_e = 6.72\%$, $R_F = 1.79\%$). The lattice parameters are $a = 6.1373(2)$ and $c = 11.4112(3)$ Å. The cross markers and the upper solid line stand for the experimental and calculated patterns, respectively. The vertical markers represent the calculated Bragg angles. The lower solid line shows the difference between the experimental and calculated intensities. The fitting parameters such as atomic positions are essentially identical to those reported for other $LnMnO_3$ compounds (4, 6, 7).

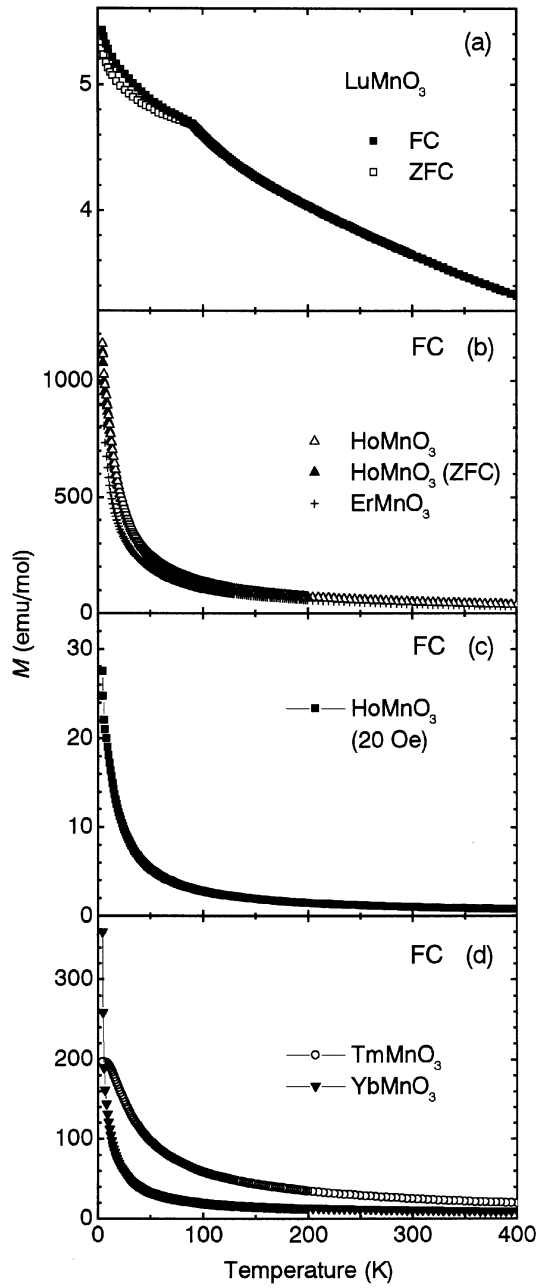

FIG. 2. (a) FC and ZFC M–T curves for $LuMnO_3$ measured with $H = 1000$ Oe. (b) FC M–T curves for $HoMnO_3$ and $ErMnO_3$ measured with $H = 1000$ Oe. A ZFC curve is shown only for $HoMnO_3$. (c) FC M–T curves for $HoMnO_3$ measured with $H = 20$ Oe. (d) FC M–T curves for $TmMnO_3$ and $YbMnO_3$ measured with $H = 1000$ Oe.

(7), and −975 K(8)). Despite the considerable deviations, it seems that the $|\theta|$ value tends to increase with decreasing ionic radius of Ln^{3+}. This is qualitatively consistent with an increase in magnetic interactions originating from the shortening of the *a*-length. The much lower T_N than $|\theta|$ is attributed to the geometrical frustration in the two-dimensional triangular Mn–O lattice (6).

Figure 2b shows the FC *M–T* curves for $HoMnO_3$ and $ErMnO_3$. It was found that their ZFC curves resembled the FC curves and exhibited slight deviation of magnetization (typically by a few percents) below T_N, as demonstrated for $HoMnO_3$. These curves provide Curie–Weiss-like profiles with no apparent magnetic transition around T_N determined by neutron diffraction, i.e., 76 K for Ln = Ho and 79 K for Ln = Er (5). This situation was true when the applied field was lowered down to 20 Oe for each compound, which is shown for $HoMnO_3$ in Fig. 2c. One explanation for this result is that these transitions are masked by the paramagnetism of Ho^{3+} (effective paramagnetic moment $\mu_{eff} = 10.6\,\mu_B$) and Er^{3+} ($\mu_{eff} = 9.6\,\mu_B$) (18). This paramagentism is plausibly enhanced by the suppression of magnetization in the Mn^{3+} sublattices due to strong antiferromagnetic interactions as is deduced from the magnetization data of $LuMnO_3$. Figure 2d shows the FC *M–T* curves for $TmMnO_3$ (T_N = 86 K (5)) and $YbMnO_3$ (T_N = 82 K(8)) measured with H = 1000 Oe. Both of the curves have profiles similar to those in Fig. 2b, exhibiting monotonic increase in magnetization with decreasing temperature. Effective paramagnetic moments of free-ion Tm^{3+} and Yb^{3+} are μ_{eff} = 7.6 and 4.5 μ_B (18), which are smaller than those of Ho^{3+} and Er^{3+}. The presence of antiferromagnetic transitions is also ambiguous in this data. For the magnetization curves reported previously for $YbMnO_3$, a paramagnetic effect of Yb^{3+} was subtracted (8). In this work, no detailed analysis for these data including the subtraction of the paramagnetic contribution of Ln^{3+} has been carried out, considering that temperature dependence of the Ln^{3+} moments cannot be accurately determined from the present data alone. The curve for $TmMnO_3$ tends to be flattened around the lowest measurement temperature of 4.5 K, probably owing to the crystal-field effect (19).

Figure 3a shows the inverse magnetization plotted against temperature for $HoMnO_3$ and $YbMnO_3$. From the CW fit above T_N, μ_P, and θ were calculated to be 11.3 μ_B/unit formula and −25 K for Ln = Ho, and 6.6 μ_B/unit formula and −200 K for Ln = Yb. These μ_P values are very close to those estimated from the free-ion Ho^{3+} and Yb^{3+} and the spin-only Mn^{3+} moments, i.e., 11.7 and 6.7 μ_B/unit formula for Ln = Ho and Yb, respectively. The absolute values of $|\theta|$ are smaller than that for $LuMnO_3$ because these θ values reflect averaged interactions of those around Mn^{3+} and Ln^{3+}. Effective internal magnetic fields acting on Ln^{3+} are plausibly much weaker than those on

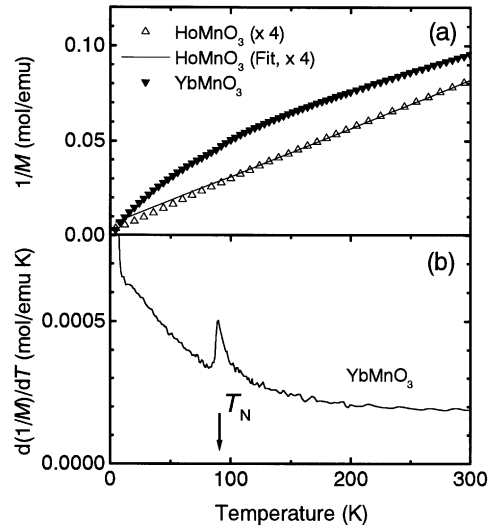

FIG. 3. (a) Inverse magnetization–temperature (1/*M–T*) curves for $HoMnO_3$ and $YbMnO_3$ obtained from Fig. 2. The Curie–Weiss fit is shown as Fit only for the $HoMnO_3$. The 1/*M* values for $HoMnO_3$ were multiplied by a factor of 4. (b) Temperature derivative of the inverse magnetization plotted against temperature for $YbMnO_3$. T_N represents the Néel temperature.

Mn^{3+}. The $|\theta|$ values for $HoMnO_3$ and $ErMnO_3$ are considerably lower than both the reported Néel temperature T_N = 76 K and 79 K (5), and T_N determined from temperature derivative shown later, suggesting that the temperature dependence of magnetization is determined mainly by the paramagnetic Ho^{3+} and Er^{3+} moments. Each curve deviates from the CW law at low temperatures, which may be understood in terms of the onset of the magnetic order of Mn^{3+}. The deviation is very slight for Ln = Ho and Er because of the large paramagnetic effect of Ln^{3+}, which is shown only for Ln = Ho in the figure. The downward deviation of the curves suggests that the magnetization is increased by spin-canting as found for $ScMnO_3$ (6,7), whose origin is assumed to be the Dzyaloshinsky–Moriya interaction (7). These qualitative characteristic features have been observed also for the other compounds. Temperature derivative of these data exhibited peak values at 76 and 88 K for Ln = Ho and Yb, respectively. This is shown in Fig. 3b only for the latter case. These temperatures could be defined as T_N. The result from both the CW fit and the temperature derivative is shown in Table 1. Each T_N is well close to the literature value (5,8). Its monotonic increase with increasing atomic number of *Ln* means the enhancement of antiferromagnetic interactions between Mn^{3+} noted earlier. Paramagnetic moments per unit formula was almost the same (~95–100%) as calculated from the free-ion Ln^{3+} and the spin-only Mn^{3+} moments. The $|\theta|$ value also increases with increasing atomic number of *Ln*. This trend could be understood in terms of the increase in magnetic

TABLE 1
Néel temperatures (T_N) and Weiss temperatures (θ) for All the LnMnO$_3$ Compounds. Each compound is expressed in terms of lanthanide (Ln) ion

Ln	T_N(K)	θ (K)
Ho	76	−25
Er	80	−30
Tm	86	−60
Yb	88	−200
Lu	90	−700

contribution of Mn^{3+}, owing to the monotonic decrease in the paramagnetic effect of Ln^{3+}.

Figure 4a shows the real part of AC susceptibility for $HoMnO_3$ measured with an AC field of 4 Oe and 800 Hz. As in the magnetization curves, temperature dependence of the susceptibility is governed mainly by the paramagnetic Ho^{3+} moment. Experimental data for all the compounds provided curve shapes analogous to those of the DC magnetization shown in Fig. 2. The imaginary part of the susceptibility in Fig. 4b decreases below ~50 K, for which a possible explanation is the combined effect of the antiferromagnetic order of the Mn^{3+} moment and a tendency toward magnetic order of Ho^{3+}. Isothermal magnetization at 4.5 K is plotted for $TmMnO_3$ in Fig. 5. No saturation magnetization with small remanance (corresponding to $1.6\times10^{-3}\,\mu_B$/formula unit) supports the existence of the antiferromagnetism. Electrical resistivity measurements below 300 K have not been successfully carried out because of very large resistance. Though the insulating behavior is observed also for LnMnO$_3$ with the larger lanthanide ions, the present poor conductivity could be attributed also to narrow band widths arising from the two-dimensionality of the Mn–O sheets.

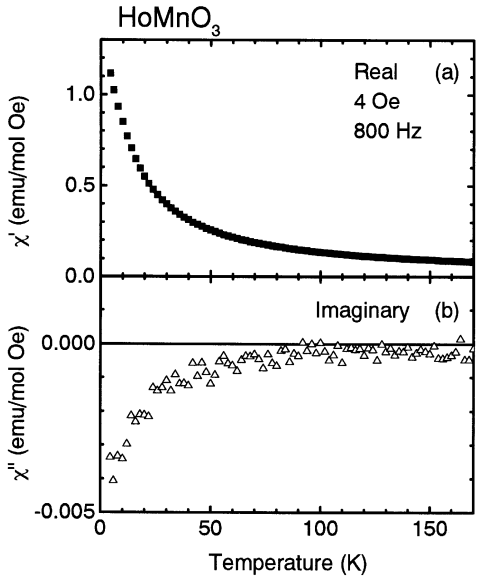

FIG. 4. (a) Real and (b) imaginary parts of AC susceptibilities for $HoMnO_3$ measured with AC field of 4 Oe and 800 Hz.

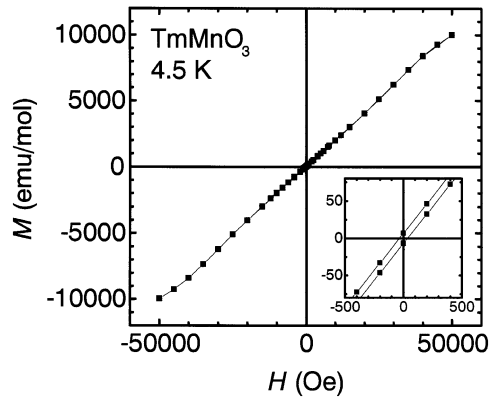

FIG. 5. Isothermal magnetization (M) at 4.5 K plotted against applied field (H) for $TmMnO_3$. The inset shows a low applied-field region.

Studies of substitution effects of the Ln^{3+} ions are currently in progress for the present compounds. As noted earlier, magnetic properties for such systems have been reported for Ca-substituted $YMnO_3$, $Y_{0.5}Ca_{0.5}MnO_3$ (11,12), and $Y_{0.7}Ca_{0.3}MnO_3$ (13). DC magnetization data are shown in Fig. 6a only for $Er_{0.5}Ca_{0.5}MnO_3$ and $Yb_{0.5}Ca_{0.5}MnO_3$ prepared by the same solid-state reaction noted in Section 2 using Ln_2O_3, Mn_2O_3, and $CaCO_3$, (3N–4N, Soekawa). The nominal valence of the Mn ion is 3.5+ in these compounds. It was found that the actual oxygen content (y) was ~2.96 for $Ln_{0.5}Ca_{0.5}MnO_{y.}$ The XRD measurements showed that the structures were orthorhombic *Pnma* ($GdFeO_3$ type) as reported for $Y_{0.5}Ca_{0.5}MnO_3$ (20). The lattice parameters calculated are $a=5.4657(3)$, $b=7.4266(6)$, $c=5.2903(5)$, and $a=5.4705(5)$, $b=7.4063(6)$, $c=5.2730(5)$ Å for $Er_{0.5}Ca_{0.5}MnO_3$, and $Yb_{0.5}Ca_{0.5}MnO_3$, respectively. The curve profiles in the figure are comparably similar to those of $ErMnO_3$ and $YbMnO_3$ (Fig. 2), showing no apparent magnetic transition, whereas low-temperature magnetization is smaller than that of LnMnO$_3$. Each ZFC curves had an analogous shape to that of the corresponding FC curve with slightly smaller magnetization (by less than ~7%) below ~70–80 K than the FC magnetization. Figure 6b shows deviation from the CW law below ~250 K for $Yb_{0.5}Ca_{0.5}MnO_3$. It is noteworthy that this temperature is close to the charge-ordering temperatures reported for some orthomanganites containing small A-site ions such as $Ln_{0.5}Ca_{0.5}MnO_3$ (Ln = Y, Pr, and Sm) (11,21). Inflection of the curve around 100 K might correspond to the short-range antiferromagnetism at 130–135 K proposed for $Y_{0.5}Ca_{0.5}MnO_3$ (11). A calculated Weiss temperature is −6 K, whose absolute value is much smaller than in $YbMnO_3$. This result suggests the contribution of a ferromagnetic double-exchange interaction generated by

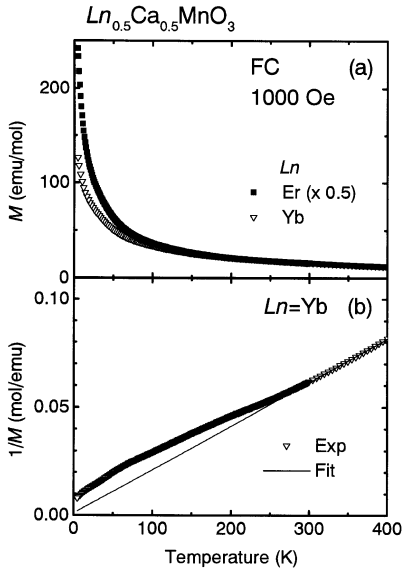

FIG. 6. (a) FC M–T curves for $Er_{0.5}Ca_{0.5}MnO_3$ and $Yb_{0.5}Ca_{0.5}MnO_3$ measured with $H = 1000$ Oe. Magnetization for $Er_{0.5}Ca_{0.5}MnO_3$ was multiplied by a factor of 0.5. (b) $1/M$-T curve for $Yb_{0.5}Ca_{0.5}MnO_3$ obtained from Fig. 6a. The experimental data and Curie–Weiss fit are labeled as Exp and Fit, respectively.

the coexistence of Mn^{3+} and Mn^{4+}. Analogous structural and magnetic properties have been obtained for all the other $Ln_{0.5}Ca_{0.5}MnO_3$. To reveal more detailed properties of the compounds shown here and their origins, further investigations such as the observation of electronic structures are under way for both LnMnO$_3$ and $Ln_{0.5}Ca_{0.5}MnO_3$.

REFERENCES

1. M. N. Iliev, H.-G. Lee, V. N. Popov, M. V. Abrashev, A. Hamed, R. L. Meng, and C. W. Chu, *Phys. Rev. B* **56,** 2488 (1997).
2. Z. Jirák, J. Hejtmánek, K. Knížek, and R. Sonntag, *J. Solid State Chem.* **132,** 98 (1997), doi:10.1006/jssc.1997.7414.
3. T. Mori, K. Aoki, N. Kamegashira, T. Shishido, and T. Fukuda, *Mater. Lett.* **42,** 387 (2000).
4. H. L. Yakel, W. C. Koehler, E. F. Bertaut, and E. F. Forrat, *Acta Crystollogr.* **16,** 957 (1963).
5. W. C. Koehler, H. L. Yakel, E. O. Wollan, and J. W. Cable, *Phys. Lett.* **9,** 93 (1964).
6. M. Bieringer, and J. E. Greedan, *J. Solid State Chem.* **143,** 132 (1999), doi:10.1006/jssc.1998.8127.
7. A. Muñoz, J. A. Alonso, M. J. Martínez-Lope, M. T. Casáis, J. L. Martínez, and M. T. Fernández-Díaz, *Phys. Rev.* B **62,** 9498 (2000).
8. T. Katsufuji, S. Mori, M. Masaki, Y. Moritomo, N. Yamamoto, and H. Takagi, *Phys. Rev. B* **64,** 104,419 (2001).
9. H. Satoh, T. Shoji, J. Iwasaki, and N. Kamegashira, *Thermochim. Acta* **261,** 47 (1995).
10. H. Satoh, J. Iwasaki K. Kawase, and N. Kamegashira, *J. Alloys Compds.* **268,** 42 (1998).
11. A. Arulraj, R. Gundakaram, A. Biswas, N. Gayathri, A. K. Raychaudhuri, and C. N. R. Rao, *J. Phys. Condens. Matter* **10,** 4447 (1998).
12. A. Arulraj, P. N. Santhosh, R. S. Gopalan, A. Guha, A. K. Raychaudhuri, N. Kumar, and C. N. R. Rao, *J. Phys. Condens. Matter* **10,** 8497 (1998).
13. R. Mathieu, P. Nordblad, D. N. H. Nam, N. X. Phuc, and N. V. Khiem, *Phys. Rev. B* **63,** 174405 (2001).
14. I. O. Troyanchuk, N. V. Samsonenko, N. V. Kasper, H. Szymczak, and A. Nabialek, *Phys. Status Solidi, A* **160,** 195 (1997).
15. M. C. Sánchez, J. Blasco, J. García, J. Stankiewicz, J. M. De Teresa, and M. R. Ibarra, *J. Solid State Chem.* **138,** 226 (1998), doi:10.1006/jssc.1998.7801.
16. W.-H. Jung, J-H. Sohn, J.-H. Lee, J.-H. Sohn, M.-S. Park, and S.-H. Cho, J. *Am. Ceram. Soc.* **83,** 797 (2000).
17. F. Izumi and T. Ikeda, *Mater. Sci. Forum* **321–324,** 198 (2000).
18. J. H. Van Vleck, "The Theory of Electric and Magnetic Susceptibilities." Oxford Univ. London, 1965.
19. E. D. Jones, *Phys. Rev.* **180,** 455 (1969).
20. D. Vega, G. Polla, A. G. Leyva, P. Konig, H. Lanza, A. Esteban, H. Aliaga, M. T. Causa, M. Tover, and B. Alascio, *J. Solid State Chem.* **156,** 458 (2001), doi:10.1006/jssc.2000.9023.
21. C. Martin, A. Maignan, M. Hervieu, and B. Raveau, *Phys. Rev. B* **60,** 12191 (1999).